This article has been accepted for publication in a future issue of this journal, but has not been fully edited. Content may change prior to final publication. Citation information: DOI 10.1109/TAP.2017.2779558, IEEE Transactions on Antennas and Propagation



# Antenna System Composed of T-shaped Elements Coupled to an Open Radial Waveguide

Hisamatsu Nakano, *Life Fellow, IEEE*, Yuhei Kameta, Toru Kawano, *Member IEEE*, Amit Mehta, *Senior Member, IEEE*, Arpan Pal, *Member IEEE*, Andrew Skippins, and Junji Yamauchi, *Fellow, IEEE*

***Abstract*—An antenna system composed of an activated open radial waveguide (RadWG) and parasitic T-shaped elements is proposed as a high-gain antenna, where the radiation beam is steerable around the system axis. The T-shaped elements are proximity-coupled to the RadWG. It is found that the upper round plate for the RadWG contributes to forming a desirable beam and increasing the gain. The beam-steering with a gain of greater than targeted 9 dBi in sixteen azimuthal directions is obtained by changing the location of open-state T-shaped elements whose height is 0.18 wavelength. Effects on the radiation characteristics of the system parameters, including the RadWG height, upper round plate diameter, ground plane diameter, and number of open-state T-shaped elements, are also analyzed and discussed.**

***Index Terms*—*T-shaped element, radial waveguide, parasitic, multidirectional beams***

## I. Introduction

An antenna system consisting of a central activated element and parasitic elements, shown in Fig. 1(a), was proposed in 1978 [1]. This system, designated as the Dipole/Dipoles, was investigated to obtain a directive beam using reactive loads attached to the parasitic elements.

The antenna systems in [2] and [3] are similar to the antenna system in [1], where parasitic elements are controlled using switching circuits instead of reactive loads. The switching circuit allows the end of the parasitic element to be open-circuited or short-circuited to the ground plane (O-state or S-state). The antenna system published in 2000 [4][5], designated as the ESPAR (Electrically Steerable Passive Array Radiator), is an extension of the antenna in [1] and is composed of parasitic elements (each has a variable reactor) and a central activated antenna. Formation of a radiation beam and a null were discussed. It was found that the gain increased when a circular ground plane with a skirt [6] was used.

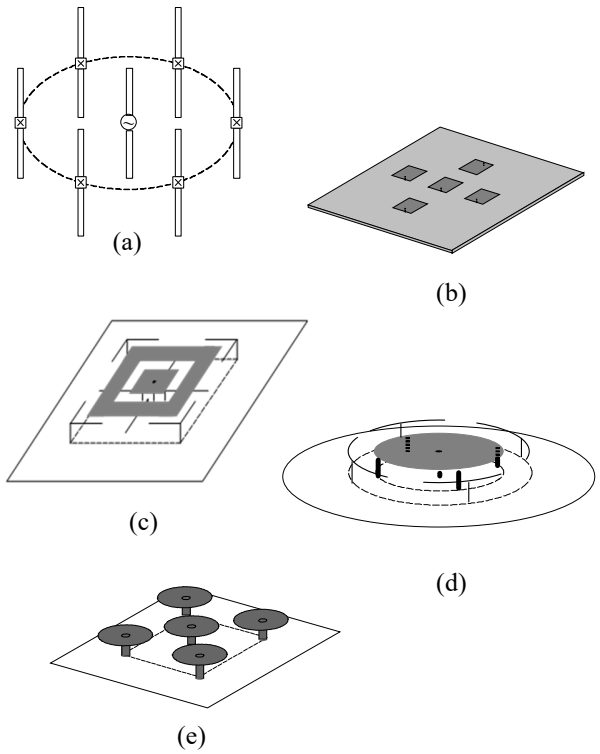


Fig. 1. Examples of conventional beam steering antenna systems (not drawn by real size). (a) Dipole/Dipoles [1]. (b) Patch/Patches [7]. (c) Patch/Ys [8]. (d) Small Shorting-Disc/Ts [9], where the upper round plate of the central fed element has a small radius of $D_{UP}/2 = 0.12$ wavelength and is shorted-circuited to the ground plane by four pins. (e) Small Mushroom/Mushrooms in [10], where the upper round plate of the central fed element has a small radius of $D_{UP}/2 \approx 0.11$ wavelength.

In addition to the abovementioned beam-steering antennas, so far, numerous beam-steerable antennas have been presented and discussed, for example, in [7]-[18].

Antennas used for modern communication systems are often required to have (i) a small antenna height of less than one-quarter wavelength ($\lambda/4$), (ii) a constant reconfigurable high gain, preferably greater than 9 dBi ( $\approx$ dipole gain + 7 dB)

Manuscript received XX XX, 2017; revised XX XX, XX; accepted XX XX, XX. Date of publication XX XX, XX; Date of current version XX XX, 2017. H. Nakano, Y. Kameta, and J. Yamauchi are with Hosei University, Koganei, Tokyo, Japan (e-mail: nakano@hosei.ac.jp). T. Kawano is with National Defense Academy, Yokosuka, Kanagawa, Japan. A. Mehta, A. Pal, and A. Skippins are with Swansea University, SA1 8EN UK (e-mail: a.mehta@swansea.ac.uk).

Color versions of one or more of the figures in this paper are available online at http://ieeexplore.ieee.org.
Digital Object Identifier 10.1109/XXX.XXXX.XXXXXXX

This article has been accepted for publication in a future issue of this journal, but has not been fully edited. Content may change prior to final publication. Citation information: DOI 10.1109/TAP.2017.2779558, IEEE Transactions on Antennas and Propagation



in multi-direction across an azimuth range of $0^o \le \phi \le 360^o$ at a fixed elevation angle $\theta$, and (iii) a simple structure that provides reconfigurable functions not using reactive loads and shifters. There is a strong need to meet these three requirements, for example, for antenna systems that are to be attached to the ceiling of a room or the roof of a vehicle.

The Dipole/Dipoles in Fig. 1(a) [1] has a height of one-half wavelength. The antenna systems using the monopoles in [2]-[6][11][12] have an antenna height of one-quarter wavelength ($\lambda/4$) or approximately $\lambda/4$. These systems do not satisfy the height criterion in (i) above.

One technique for reducing the antenna height is to fold the parasitic elements, as shown in Fig. 2 in [13] and Fig. 1 in [14]. However, the gain for these antenna systems is low (less than 5 dBi) and does not meet the targeted gain requirement in (ii). A low gain is also a characteristic of the Patch/Patches in Fig. 1(b) [7], the Patch/Ys in Fig. 1(c) [8], the Small Shorting-Disc/Ts in Fig. 1(d) [9], and the array in [10], although the small antenna height requirement in (i) is met. Note that antennas in [15]-[18] adopt microstrip structures and meet the small antenna height requirement, but they do not fulfill the targeted gain requirement across the desired beam-steering range.

To our best knowledge, there have not been high-gain beam-steerable/reconfigurable antennas for multi-azimuthal directions with a small antenna height of less than $\lambda/4$. From this, this paper proposes a novel antenna system composed of an open radial waveguide and T-shaped parasitic elements with small height, O-RadWG/Ts, where electromagnetic proximity-coupling (EM-ProxCoP) is used between the edge of the open radial waveguide and the parasitic T-shaped elements. The novel antenna system obviously differs from reconfigurable antenna systems that use "free-space coupling" to excite several parasitic elements by a central activated element [a representative example is shown in Fig. 1(a)]. In addition, the novel antenna has a high-gain reconfigurable function in 16 directions without attaching reactive loads and phase shifters to parasitic elements.

One comment is made here, focusing on an inner section constituting the Small Shorting-Disc/Ts in Fig. 1(d), which we created in 2006 [9]. This inner section is made of a pin-shorted small disc (radius $D_{UP}/2$) fed by a central monopole, designated as the Small Shorting-Disc Monopole Antenna. Fig. 26 in Appendix shows the radiation pattern, VSWR, and directivity for the Small Shorting-Disc Monopole Antenna as a function of the radius of an upper round plate, $D_{UP}/2$. The VSWR is changed with a change in $D_{UP}/2$, but the radiation pattern (and hence directivity) is almost unchanged. Note that, when $D_{UP}/2 = 0$, the Small Shorting-Disc Monopole Antenna becomes a simple isolated monopole without an upper round plate and four pins. It is found that the Small Shorting-Disc Monopole Antenna almost maintains the radiation pattern and directivity for the simple isolated monopole ($D_{UP}/2 = 0$). This means that the upper round plate less contributes to forming the radiation pattern (and hence the directivity). In other words, the current on the small upper round plate (radius of 0.12 wavelength in [9]) is not a major source to form the radiation. Note that this kind of almost unchanged radiation pattern (and hence almost unchanged directivity) is also found in the activated central antenna with the top-loading small disc shown in Fig. 1(e) [10].

In contrast, the newly proposed O-RadWG/Ts in this paper does not use pin-shorted disc unlike the Small Shorting-Disc/Ts in Fig. 1(d). In addition, the upper round plate for the O-RadWG/Ts has a large radius (of $D_{UP}/2 \approx$ half the wavelength, forming an O-RadWG) and is used to constructively form a desirable radiation pattern that leads to high gain, not obtained by the conventional antenna in Fig. 1(d). The O-RadWG/Ts can steer the beam in multi-direction (16 directions) with reconfigurability in the radiation pattern, gain, and VSWR. The antenna structure (with an open radial waveguide, not a small disc), design concept, and radiation pattern formation for the O-RadWG/Ts differ from those for the antennas in [9][10]. Realization or possibility of forming 16 reconfigurable beams has not been discussed in [9][10] (which have basically 4 beams).

This paper consists of seven sections. Section II shows the design procedure and mechanism of a proposed reconfigurable antenna system. Section III illustrates an evolution from a conventional free-space coupling beam-steering antenna to a novel EM-ProxCoP beam-steering antenna, where sixteen T-shaped parasitic elements surround a central activated antenna element. The role of the large upper round plate for the EM-ProxCoP is clarified using the N4 integral equation [19] with the method of moments (MoM) [20] and an EM simulation solver based on a finite integration technique (FIT) [21]. Section IV reveals the effects of the configuration parameters on the O-RadWG/Ts antenna characteristics. Based on the parameter study in section IV, a sixteen-direction beam-steering O-RadWG/Ts system is fabricated and measured in section V. Section VI summarizes the state of T-shaped elements for sixteen steered beams. Finally, section VII summarizes the obtained results on the O-RadWG/Ts.

## II. Design Process and Radiation Mechanism

For a unidirectional steerable beam in the azimuth direction ranging from $\phi = 0^o$ to $360^o$, a circular array system is adopted. Fig. 2 shows a system composed of $N_{ac}$ elements [$N_{ac} = (2m+1)$: m = 1,2, …], where one element is on the negative x-axis. These elements, each having dimension $T_{VER}$ in the vertical direction (z-direction) and dimension

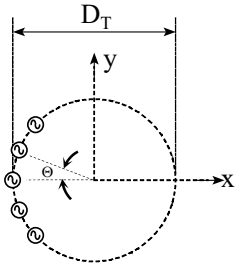


Fig. 2. Array of 2m + 1 elements.

This article has been accepted for publication in a future issue of this journal, but has not been fully edited. Content may change prior to final publication. Citation information: DOI 10.1109/TAP.2017.2779558, IEEE Transactions on Antennas and Propagation



$2T_{HOR}$ in the horizontal direction, are resonant-type elements and located on a circle of radius $D_T/2$ in the x-y plane (ground plane GP). The space angle between neighboring elements is uniform and denoted as $\Theta$. The elements are activated in phase with the same amplitude.

The first step in the system design is to calculate the array factor pattern in the x-y plane of Fig. 2 with the number of activated elements $N_{ac}$ as a parameter. For this, the radius of array circle $D_T/2$ and the space angle $\Theta$ are chosen to be $D_T/2 > \lambda/2$ and $\Theta > 2T_{HOR}/(D_T/2)$, where $\lambda$ denotes the wavelength at the design frequency. The choice of $D_T/2$ will be understood in the second step. By the freedom of space angle $\Theta$, neighboring activated elements avoid physical contact.

From the calculated array factor patterns (see Fig. 25, an example in Appendix), the number of array elements that provides a narrow bidirectional pattern in the ±x-direction, $N_{ac} \equiv N_{op}$, is determined, which is needed to realize high gain. Note that the bidirectional pattern is changed to a unidirectional pattern toward the negative x-direction through the following step.

In the second step, the antenna system in Fig. 2 is modified to an antenna system shown in Fig. 3(a), where one large element is newly introduced, which occupies a shadowed area. This introduced element is activated by a central z-directed wire at the coordinate origin, while the previously activated $N_{op}$ elements are changed to non-activated elements (indicated by white dots). Note that these non-activated elements are indirectly excited by the new central activated element through electromagnetic proximity-coupling (EM-ProxCoP). For EM-ProxCoP, radial transmission lines [see Fig. 4(b)], a grid plate [see Fig. 4(c)], and an open radial waveguide [see Fig. 4(d)] are good candidates, because these structures facilitate the EM-ProxCoP to the $N_{op}$ non-activated elements through small gap, $\Delta g$. The radius of these structures, denoted as $D_{UP}/2$, is chosen to be large so that a large current is distributed on the upper surface of the structures. This surface current is used for improving the radiation pattern. A value of approximately $\lambda/2$ is a good choice for $D_{UP}/2$, on the basis of resonance. Thus, $D_{UP}/2 + \Delta g = D_T/2 > \lambda/2$, as mentioned in step I.

Furthermore, as shown in Fig. 3(b), $N_{sh}$ parasitic elements indicated by cross marks are added behind the indirectly excited $N_{op}$ elements, with space angle $\Theta$. Thus, $\Theta = 2\pi/M_T$, satisfying $\Theta > 2T_{HOR}/(D_T/2)$, where $M_T \equiv N_{op} + N_{sh}$. The structure of the $N_{sh}$ parasitic elements is the same as that of the $N_{op}$ non-activated elements. However, the state of the bottom end of the $N_{sh}$ elements (short-circuited to a ground plane, S-state, as will be described in section III) differs from that of $N_{op}$ elements (open-circuited to a ground plane, O-state, as will be described section III). These $N_{sh}$ parasitic elements act as reflector-function elements for the $N_{op}$ elements, thereby changing the bidirectional radiation into unidirectional radiation toward the negative x-direction. Consequently, a high gain beam is obtained.

Note that the antenna structure is symmetric with respect to the z-axis. Therefore, a high gain beam can be steered in $M_T$ directions by changing the position of consecutive $N_{op}$ O-state elements and the remaining $N_{sh}$ S-state elements. This will be more clearly shown later in section VI.

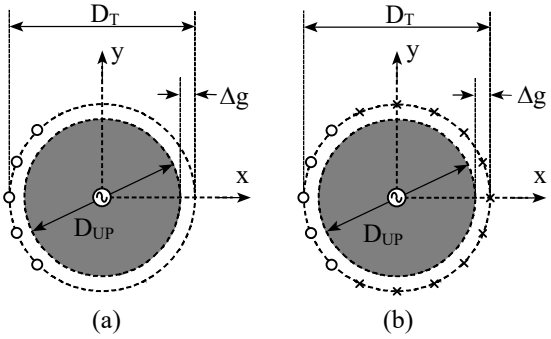


Fig. 3. Conceptual array for realizing a negative x-directed unidirectional beam. (a) $N_{op}$ non-activated elements denoted by white dots and one activated element illustrated by a shadowed area, which is fed by a central z-directed wire. (b) Addition of $N_{sh}$ parasitic elements, denoted by cross marks (x). All elements on the circle of diameter $D_T$ have the same structure. The bottom end is in O-state for the $N_{op}$ elements and S-state for the $N_{sh}$ elements.

## III. Evolution To Open Radial Waveguide With T-Shaped Elemnts (O-RadWG/Ts)

Based on the discussion in section II, the radial structure is embodied. For better understanding of the O-RadWG/Ts, Fig. 4 shows an evolution from a space-coupling beam steerable Monopole/Ts to an electromagnetic proximity-coupling O-RadWG/Ts through Radial-Lines/Ts and Grid-Plate/Ts. There are T-shaped elements surrounding a central activated element, which is a monopole in Fig. 4(a), a bundle of radial transmission lines in Fig. 4(b), a grid plate in Fig. 4(c), and an open radial waveguide in Fig. 4(d). The grid plate for the Grid-Plate/Ts is an extension of the bundle of radial transmission lines for the Radial-Lines/Ts. The O-RadWG/Ts is an extension of the Grid-Plate/Ts.

The T-shaped sixteen elements ($M_T = 16$) are circularly arrayed with a radius of $D_T/2 = 37$ mm $= 0.52\lambda_{4.2}$ and a space angle of $\Theta = 22.5^o$ on a ground plane, GP, where $\lambda_{4.2}$ is the free-space wavelength at a design frequency of 4.2 GHz. The T-shaped parasitic element has a vertical length of $T_{VER} = 13$ mm $= 0.18\lambda_{4.2} < \lambda_{4.2}/4$ and a horizontal length of $2T_{HOR} = 10$ mm, leading to $T_{VER} + T_{HOR} = 18$ mm $\approx \lambda_{4.2}/4$. The antenna height of $H = 13$ mm $= 0.18\lambda_{4.2}$ equals $T_{VER}$. The upper sections of the radial transmission lines, grid plate, and radial waveguide have a radius of $D_{UP}/2 = 35$ mm $= 0.49\lambda_{4.2}$. A gap of $\Delta g = 2$ mm is used between the activated element and T-shaped elements in Figs. 4(b)-(d). The wires constituting the antenna systems are thin: $2a_F = 1.7$ mm $= 0.0238\lambda_{4.2}$ and $2a_T = 1.4$ mm $= 0.0196\lambda_{4.2}$.

This article has been accepted for publication in a future issue of this journal, but has not been fully edited. Content may change prior to final publication. Citation information: DOI 10.1109/TAP.2017.2779558, IEEE Transactions on Antennas and Propagation



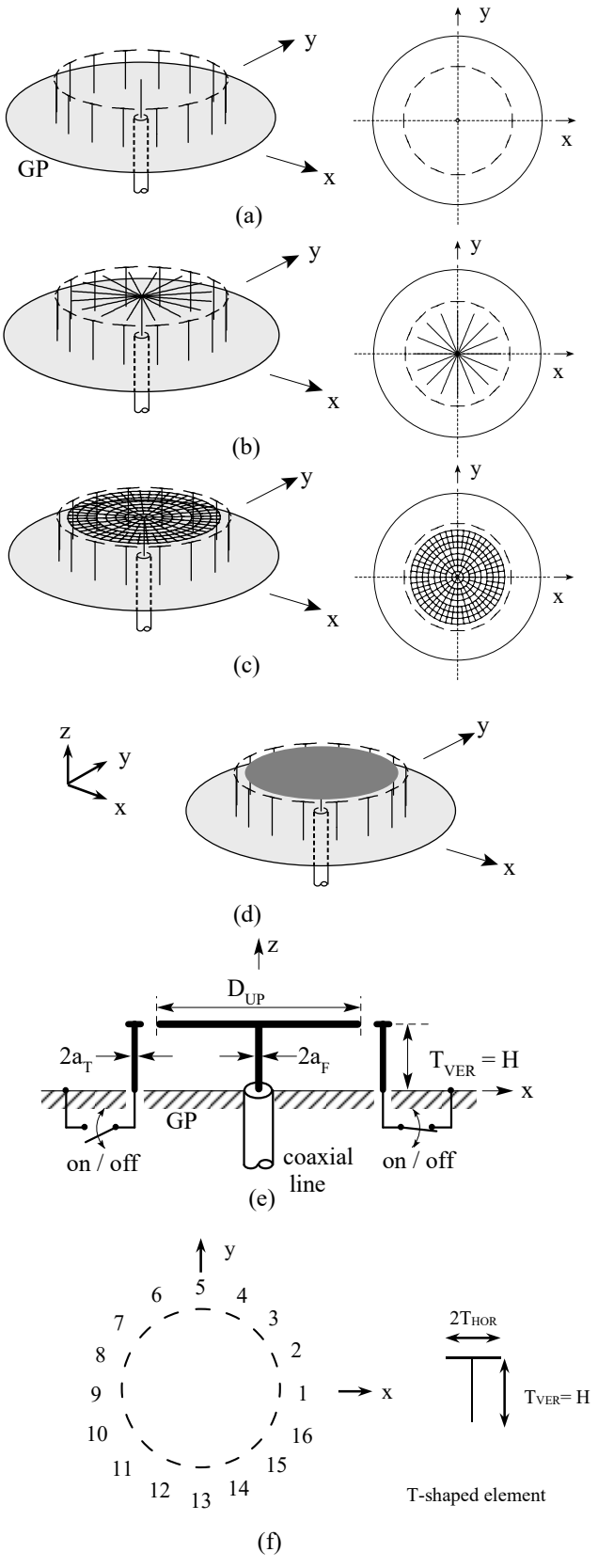


Fig. 4. Four antenna systems. (a) Monopole/Ts. (b) Radial-Lines/Ts. (c) Grid-Plate/Ts. (d) O-RadWG/Ts. (e) Side view for Radial-Lines/Ts, Grid-Plate/Ts, and O-RadWG/Ts, where $D_{UP}$ denotes the diameter of the upper section for these antenna systems. (f) Numbering of T-shaped elements.

The following *subsection A* presents the radiation pattern for the O-RadWG/Ts, comparing those for the other three antenna systems. Subsequently, *subsections B* and *C* reveal the effects of the upper round plate for the O-RadWG/Ts on the radiation pattern, gain, and VSWR.

### *A. Radiation patterns*

Fig. 5 shows the radiation pattern for the O-RadWG/Ts, together with those for other three antenna systems, where the bottom end of T-shaped five elements 7, 8, 9, 10, and 11 is open-circuited to the ground plane (O-state) and the remaining eleven T-shaped elements are short-circuited to the ground plane (S-state): $N_{op}$ = 5 and $N_{sh}$ = 11. These numbers $N_{op}$ and $N_{sh}$ are determined, based on the design process in section II. The analysis/simulation is performed using the method of moments (MoM) [20] with the N4 integral equation [19] and the FIT (Finite Integration Technique) [21], where the ground plane is assumed to be of infinite extent. It is found that all antenna systems form the radiation beam in the negative x-direction.

The radiation pattern for the Grid-Plate/Ts is found to be almost the same as that for the O-RadWG/Ts with a gain of greater than the targeted gain 9 dBi. This means that the upper round plate for the open radial waveguide can be approximated by the grid plate, and the analysis/simulation results for the Grid-Plate/Ts are very close to those for the O-RadWG/Ts.

### *B. Contribution of the upper round plate for the O-RadWG/Ts to the radiation pattern*

It is worth investigating how the total radiation field in Fig. 5(d) is formed by the antenna system elements. For this, two partial radiation fields are calculated using the currents obtained from the MoM analysis; one is the partial radiation field from the upper round plate for the O-RadWG/Ts, $\mathbf{E}_{UP}$, and the other is the partial radiation field from the compound of the central monopole and the T-shaped elements, $\mathbf{E}_{M+T}$. The total radiation field, $\mathbf{E}$, is the vector sum of $\mathbf{E}_{UP}$ and $\mathbf{E}_{M+T}$, i.e., $\mathbf{E} = \mathbf{E}_{UP} + \mathbf{E}_{M+T}$.

Fig. 6(a) shows the partial radiation field $\mathbf{E}_{UP}$, and Fig. 6(b) shows the partial radiation field $\mathbf{E}_{M+T}$. For convenience, the radiation field in Fig. 5(d) is again shown in Fig. 6(c), as the total radiation field $\mathbf{E}$. It is found that $\mathbf{E}_{M+T}$ is similar to $\mathbf{E}$. This means that a basis for the total radiation field is $\mathbf{E}_{M+T}$, i.e., the partial radiation field from the compound of the central monopole and T-shaped elements.

Note that $\mathbf{E}_{M+T}$ in Fig. 6(b) differs from the radiation field shown in Fig. 5(a), although both the structures are the same.

This article has been accepted for publication in a future issue of this journal, but has not been fully edited. Content may change prior to final publication. Citation information: DOI 10.1109/TAP.2017.2779558, IEEE Transactions on Antennas and Propagation



This is due to the presence of the upper round plate, which changes the initial current distribution along the central monopole and the T-shaped parasitic elements shown in Fig. 5(a).

The partial radiation field from the upper round plate, $\mathbf{E}_{UP}$, plays an important role in forming $\mathbf{E}$. In order to clarify the role of the upper round plate, we focus on the field intensity in the $\theta = 30^o$ direction of the x-z elevation plane with $x > 0$; a side lobe exists, as shown in the x-z plane of Figs. 6(b) and (c). The side lobe in the dominant partial radiation field $\mathbf{E}_{M+T}$ of Fig. 6(b) is approximately – 3 dB, while the side lobe in the total radiation field $\mathbf{E}$ in Fig. 6(c) is less than – 10 dB, due to the presence of the upper round plate.

The reduction/improvement to a value of less than – 10 dB is attributed to the following fact. The phase of $\mathbf{E}_{M+T}$ in the $\theta = 30^o$ direction is – 68.1°, while the phase of $\mathbf{E}_{UP}$ in the same direction is – 241.3°. Hence, the difference between these phases is 173.2°, which is close to 180 degrees. This means that $|\mathbf{E}| = |\mathbf{E}_{UP} + \mathbf{E}_{M+T}| < |\mathbf{E}_{M+T}|$ in the $\theta = 30^o$ direction, leading to a reduced side lobe in the total radiation pattern. It follows that the upper round plate contributes to side lobe reduction.

A similar reduction occurs in the 30° direction of the x-z elevation plane with $x < 0$. The phase of $\mathbf{E}_{M+T}$ is 32.9°, and the phase of $\mathbf{E}_{UP}$ is −109.2°. As a result, the total radiation, $|\mathbf{E}_{UP} + \mathbf{E}_{M+T}|$, becomes smaller than the dominant partial radiation, $|\mathbf{E}_{M+T}|$, i.e., $|\mathbf{E}| = |\mathbf{E}_{UP} + \mathbf{E}_{M+T}| < |\mathbf{E}_{M+T}|$ in the $\theta = 30^o$ direction.

Note that the elevation-plane radiation pattern for the O-RadWG/Ts in Fig. 6(c) is narrower, compared with that for the Monopole/Ts (conventional structure) in Fig. 5(a), where the upper round plate is absent. The narrower radiation pattern for the O-RadWG/Ts becomes a factor that leads to a higher gain, compared with the gain for the Monopole/Ts.

Further contribution of the upper round plate is found in the azimuth-plane radiation pattern. The azimuth-plane radiation pattern in Fig. 6(c) for the O-RadWG/Ts has a narrower beam width than that in Fig. 5(a) for the Monopole/Ts (which has no upper round plate). This comparison straightforwardly illustrates that the narrowness is caused by the upper round plate.

This section has shown that the upper round plate, which is newly introduced into the Monopole/Ts in Fig. 4(a) to construct the O-RadWG/Ts in Fig. 4(d), contributes to reducing the side lobe level in the elevation plane and narrowing the beam width in both the elevation and azimuth planes. Note that the same results regarding the radiation pattern are obtained for the Grid-Plate/Ts.

### *C. Contribution of the upper round plate for the O-RadWG/Ts to the gain and VSWR.*

As mentioned in *subsection B*, the radiation pattern is improved by the upper round plate. From this, we can infer an increase in the gain.

In order to clarify the effect of the upper round plate on the gain, Fig. 7 shows a comparison of the frequency response of the gains for the O-RadWG/Ts and the Monopole/Ts resulting from the removal of the upper round plate from the O-

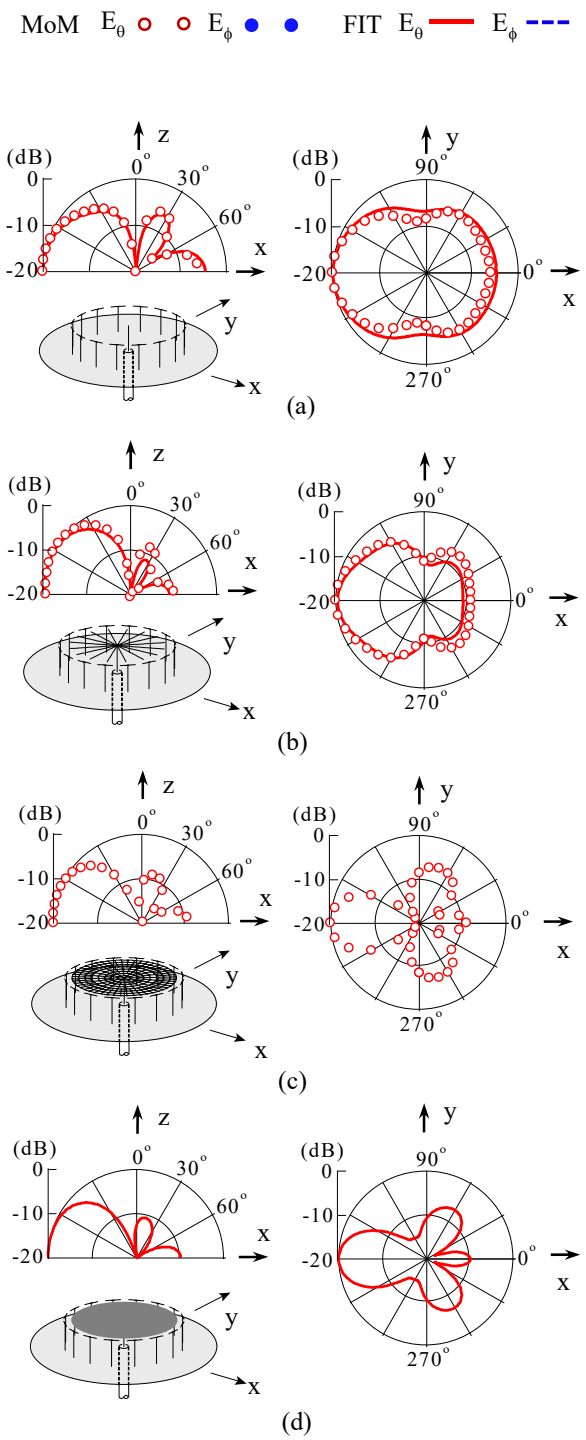


Fig. 5. Radiation patterns of four antenna systems at 4.2 GHz. The ground plane is of infinite extent. $E_\phi$ does not appear. (a) Monopole/Ts. (b) Radial-Lines/Ts. (c) Grid-Plate/Ts, where a grid cell has a length of $\leq$ 4.57 mm = $0.064\lambda_{4.2}$ in the azimuthal direction and a length of $\leq$ 4.38 mm = $0.061\lambda_{4.2}$ in the radial direction. (d) O-RadWG/Ts.

This article has been accepted for publication in a future issue of this journal, but has not been fully edited. Content may change prior to final publication. Citation information: DOI 10.1109/TAP.2017.2779558, IEEE Transactions on Antennas and Propagation



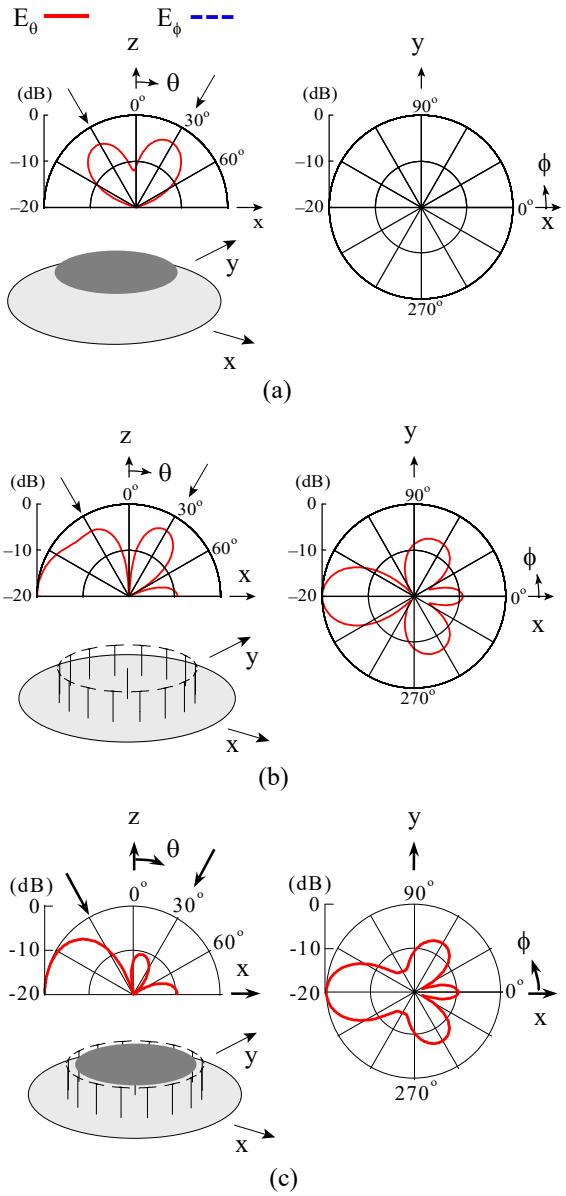


Fig. 6. Radiation decomposition at 4.2 GHz. The ground plane is of infinite extent. $E_\phi$ does not appear. (a) Partial radiation field from the upper round plate for the O-RadWG/Ts, $\mathbf{E}_{UP}$. (b) Partial radiation field from the compound of the activated monopole and T-shaped elements, $\mathbf{E}_{M+T}$. (c) Total radiation field $\mathbf{E}$.

RadWG/Ts. The comparison reveals that the upper round plate has a constructive effect on the gain at the design frequency of 4.2 GHz. The gain in the beam direction (the negative x-direction) is greater than the targeted gain 9 dBi at the design frequency, which is approximately 2 dB higher than the gain for the Monopole/Ts in Fig. 5(a).

Analysis/simulation is also devoted to revealing the effect of the upper round plate for the O-RadWG/Ts on the input characteristic in terms of the VSWR. Fig. 8 shows a

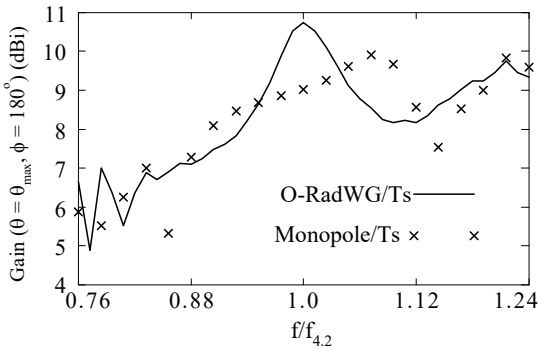


Fig. 7. Frequency response of the gains for the O-RadWG/Ts and the Monopole/Ts resulting from the removal of the upper round plate from the O-RadWG/Ts. The ground plane is of infinite extent. Notation $f_{4.2}$ denotes 4.2 GHz.

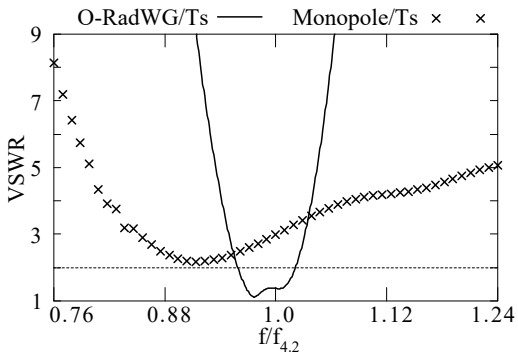


Fig. 8. Frequency response of the VSWRs for the O-RadWG/Ts and the Monopole/Ts resulting from the removal of the upper round plate from the O-RadWG/Ts. The ground plane is of infinite extent. Notation $f_{4.2}$ denotes 4.2 GHz.

comparison of the VSWR frequency responses for the O-RadWG/Ts and the Monopole/Ts resulting from the removal of the upper round plate from the O-RadWG/Ts. It is clear that the upper round plate contributes an improvement in the VSWR at frequencies around the design frequency of 4.2 GHz. Note that the same analysis/simulation results are obtained for the Grid-Plate/Ts.

Thus, contributions of the upper round plate to the radiation pattern, gain, and VSWR have been clarified, where a technique of EM-ProxCoP (electromagnetic proximity-coupling) is used between the radial waveguide and T elements.

## IV. Parameter Study for The O-RadWG/Ts

We investigate the effects of the O-RadWG/Ts structural parameters on the antenna characteristics.

The horizontal section of the T-shaped element in this section is made of a conducting strip of width w and length $2T_{HOR}$, as shown in Fig. 9, for easiness of fabrication. The parameters fixed throughout this section are presented in Table I,

This article has been accepted for publication in a future issue of this journal, but has not been fully edited. Content may change prior to final publication. Citation information: DOI 10.1109/TAP.2017.2779558, IEEE Transactions on Antennas and Propagation



where $M_T$ denotes the total number of T-shaped elements, as denoted in section II: $M_T = N_{op} + N_{sh}$.

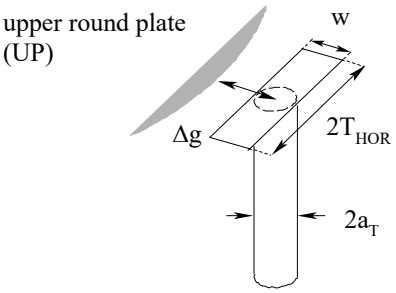


Fig. 9. T-shaped element for the O-RadWG/Ts.

TABLE I. PRIMARY PARAMETERS

| Symbol | Value | Symbol | Value | Symbol | Value |
|---|---|---|---|---|---|
| $2a_T$ | 1.4 mm | Δg | 2 mm | w | 1.4 mm |
| $M_T$ | 16 | $2a_F$ | 1.7 mm | | |

The parameters ($H = T_{VER}$, $T_{HOR}$, $D_{GP}$, $D_{UP}$, $N_{op}$) are varied subject to the objectives of the analysis/simulation, where H is the antenna height, already defined in Fig. 4(e), which equals the height of the T-shaped element $T_{VER}$; $D_{GP}$ and $D_{UP}$ denote the ground plane diameter and the upper round plate diameter, respectively. Note that $2a_F$ denotes the diameter of the center wire feeding the radial waveguide, as defined in Fig. 4(e).

### *A. Antenna height H*

We reveal the effects of antenna height $H = T_{VER}$ on the antenna characteristics. In this subsection, the upper round plate diameter is fixed to be $D_{UP} = 70$ mm and the ground plane diameter is assumed to be of infinite extent: $D_{GP} = \infty$. The bottom end of T-shaped elements (7, 8, 9, 10, 11) is open-circuited ($N_{op} = 5$) and the bottom end of the remaining T-shaped elements is short-circuited to the ground plane ($N_{sh} = 11$). This situation is summarized as ($H = T_{VER}$, $T_{HOR}$, $D_{UP}$, $D_{GP}$, $N_{op}$) = (varied, varied by 18 mm – H, 70 mm, $\infty$, 5). Fig. 10 shows the VSWR frequency response. It is found that the VSWR has a bandwidth of approximately 6%. Note that a height of H = 18 mm corresponds to $\lambda_{4.2}/4$, where the horizontal section of the T-shaped element does not exist (i.e., length $2T_{HOR} = 0$), hence the T-shaped element has a simple pole structure.

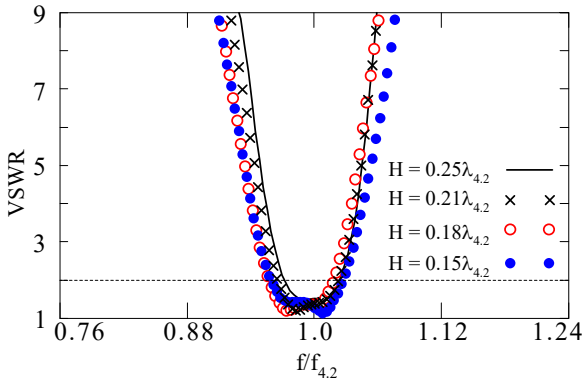


Fig.10. Frequency response of the VSWR with antenna height H as a parameter, where $f_{4.2} = 4.2$ GHz and $\lambda_{4.2} = 71.43$ mm. Parameters ($H = T_{VER}$, $T_{HOR}$, $D_{UP}$, $D_{GP}$, $N_{op}$) = (varied, varied by 18 mm – H, 70 mm, $\infty$, 5) are used, together with the parameters in Table I. The bottom end of five T-shaped elements (7, 8, 9, 10, 11) is open-circuited.

The change in the radiation pattern is shown in Fig.11. The radiation in the x-z elevation plane has a maximum intensity in the negative x-direction, with similarly shaped radiation patterns for the different heights. The radiation in the x-y azimuth plane is also found to have a maximum intensity in the negative x-direction. There is no abrupt change in the azimuth-plane radiation with change in antenna height H; no abrupt change is held for the elevation-plane radiation.

### *B. Upper round plate diameter $D_{UP}$*

Effects of the radial waveguide on the antenna characteristics are investigated with the upper round plate diameter, $D_{UP}$, as a parameter. For this, $H = T_{VER} = 13$ mm $= 0.18\lambda_{4.2}$ and $T_{HOR} = H - T_{VER} = 5$ mm $= 0.07\lambda_{4.2}$ are chosen, based on the results in Figs. 10 and 11. Thus, the parameters ($H = T_{VER}$, $T_{HOR}$, $D_{UP}$, $D_{GP}$, $N_{op}$) = (13 mm, 5 mm, varied, $\infty$, 5) are used for an antenna system with T-shaped elements (7, 8, 9, 10, 11) in O-state and the parameters in Table I.

Figs. 12(a) and (b) show the frequency response of the gain and VSWR, respectively. It is found that the maximum gain at a frequency of greater than or equal to 4.2 GHz exceeds the targeted gain 9 dBi. It is also found that, as the upper round plate becomes larger, the minimum-VSWR frequency, at which $D_{UP}$ is approximately one wavelength, becomes lower. It is desired that the maximum gain be within the VSWR bandwidth. This happens for $D_{UP} = 70$ mm $= 0.98\lambda_{4.2}$.

### *C. Ground plane diameter $D_{GP}$*

The investigation in *subsections A* and *B* is performed assuming that the ground plane is of infinite extent: $D_{GP} = \infty$. This subsection investigates how the ground plane affects the

This article has been accepted for publication in a future issue of this journal, but has not been fully edited. Content may change prior to final publication. Citation information: DOI 10.1109/TAP.2017.2779558, IEEE Transactions on Antennas and Propagation



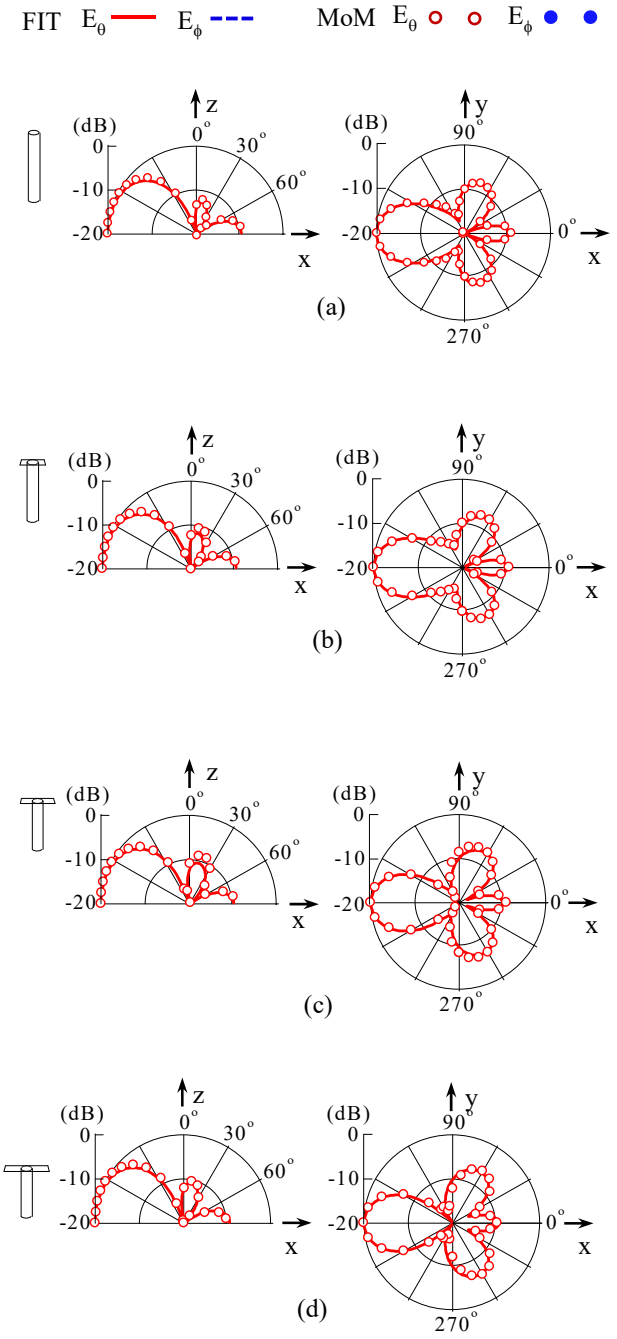


Fig. 11. Radiation patterns at 4.2 GHz with antenna height H as a parameter. Parameters (H = $T_{VER}$, $T_{HOR}$, $D_{UP}$, $D_{GP}$, $N_{op}$) = (varied, varied by 18 mm – H, 70 mm, ∞, 5) are used, together with the parameters in Table I. The bottom end of T-shaped elements (7, 8, 9, 10, 11) is open-circuited. $E_\phi$ does not appear. (a) H = 18 mm ≈ $\lambda_{4.2}/4$. (b) H = 15 mm = 0.21$\lambda_{4.2}$. (c) H = 13 mm = 0.18$\lambda_{4.2}$. (d) H = 11 mm = 0.15$\lambda_{4.2}$.

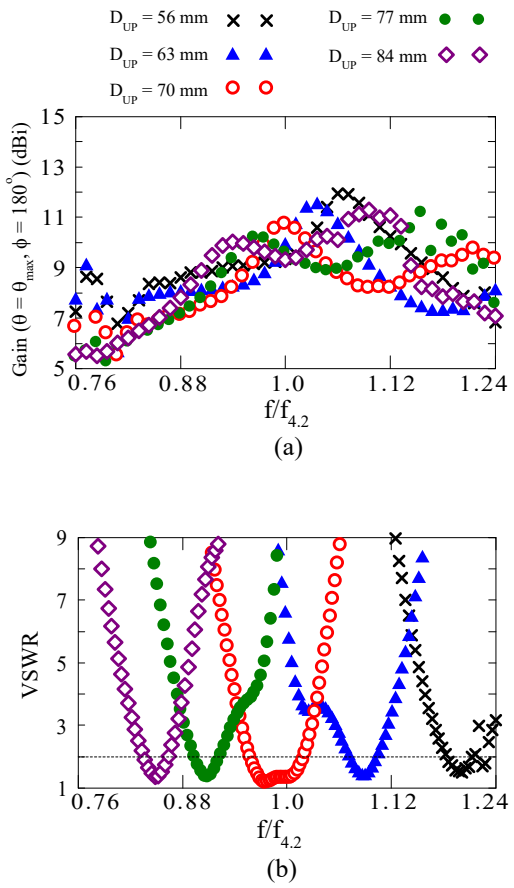


Fig. 12. Effects of the upper round plate diameter $D_{UP}$. Parameters (H = $T_{VER}$, $T_{HOR}$, $D_{UP}$, $D_{GP}$, $N_{op}$) = (13 mm, 5 mm, varied, ∞, 5) are used, together with the parameters in Table I. The bottom end of T-shaped elements (7, 8, 9, 10, 11) is open-circuited. (a) Gain. (b) VSWR.

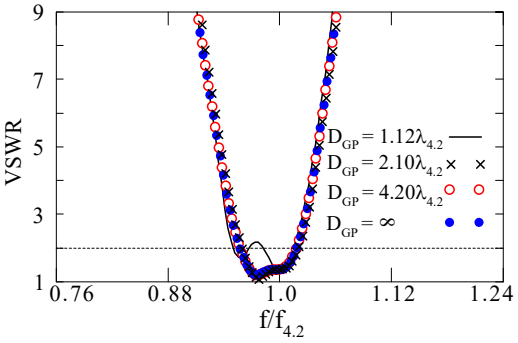


Fig. 13. Frequency response of the VSWR with ground plane diameter $D_{GP}$ as a parameter. Parameters (H = $T_{VER}$, $T_{HOR}$, $D_{UP}$, $D_{GP}$, $N_{op}$) = (13 mm, 5 mm, 70 mm, varied, 5) are used, together with the parameters in Table I. The bottom end of T-shaped elements (7, 8, 9, 10, 11) is open-circuited.

This article has been accepted for publication in a future issue of this journal, but has not been fully edited. Content may change prior to final publication. Citation information: DOI 10.1109/TAP.2017.2779558, IEEE Transactions on Antennas and Propagation



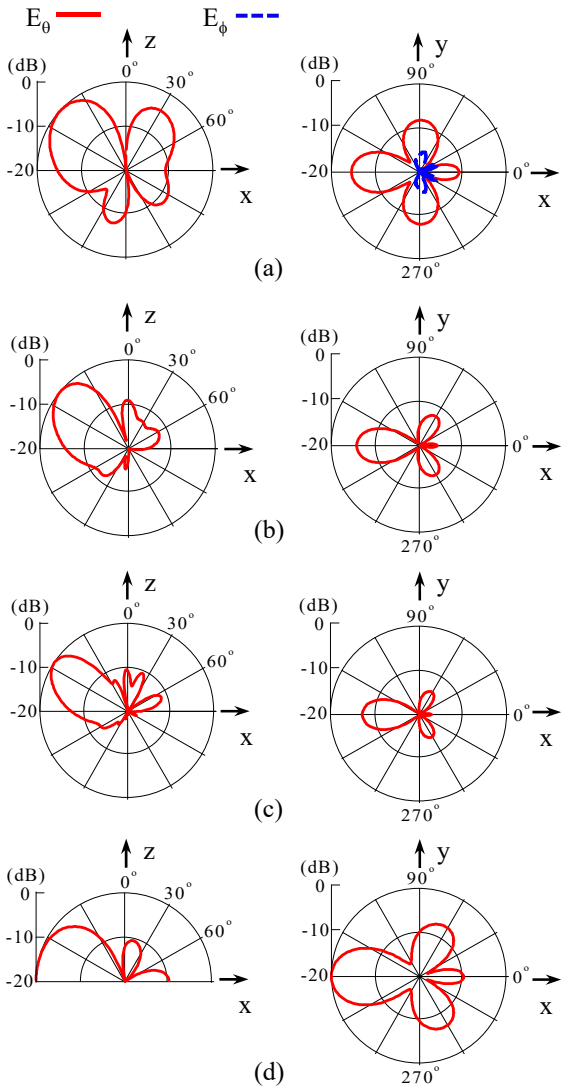


Fig. 14. Radiation patterns at 4.2 GHz ($\lambda_{4.2}$ = 71.43 mm), with ground plane diameter $D_{GP}$ as a parameter. Parameters (H = $T_{VER}$, $T_{HOR}$, $D_{UP}$, $D_{GP}$, $N_{op}$) = (13 mm, 5 mm, 70 mm, varied, 5) are used, together with the parameters in Table I. The bottom end of five T-shaped elements (7, 8, 9, 10, 11) is open-circuited. (a) $D_{GP}$ = 80 mm = 1.12$\lambda_{4.2}$. (b) $D_{GP}$ = 150 mm = 2.10$\lambda_{4.2}$. (c) $D_{GP}$ = 300 mm = 4.20$\lambda_{4.2}$. (d) $D_{GP}$ = ∞.

antenna characteristics, using parameters (H = $T_{VER}$, $T_{HOR}$, $D_{UP}$, $D_{GP}$, $N_{op}$) = (13 mm, 5 mm, 70 mm, varied, 5) and the parameters in Table I, with O-state T-shaped elements (7, 8, 9, 10, 11). Note that the value of the upper round plate diameter, $D_{UP}$ = 70 mm, is chosen from the result in *subsection B*.

As shown in Fig. 13, the VSWR values are very close to the VSWR for a ground plane of infinite extent. However, as seen from Fig. 14, the radiation pattern in the x-z elevation plane is remarkably changed by the diffraction caused by the finiteness of the ground plane. As the ground plane diameter $D_{GP}$ is increased, the beam direction shifts toward the horizontal plane. Note that the direction of the maximum radiation in the x-y azimuth plane remains unchanged, i.e., always in the negative x-direction.

### *D. Number of O-state T-shaped elements, $N_{op}$*

Fig. 15 shows the radiation pattern in the x-y azimuth plane when the number of open-state T-shaped elements, $N_{op}$, is changed. The parameters for this case are as follows: (H = $T_{VER}$, $T_{HOR}$, $D_{UP}$, $D_{GP}$, $N_{op}$) = (13 mm, 5 mm, 70 mm, 150 mm, varied) and the parameters in Table I, where $D_{GP}$ = 150 mm is chosen from *subsection C*. Table II shows the state of the T-shaped elements; "O" and "S" denote that the end of the T-shaped element is open-circuited (O-state) and short-circuited (S-state), respectively. $N_{op}$ = 0 describes a situation where all

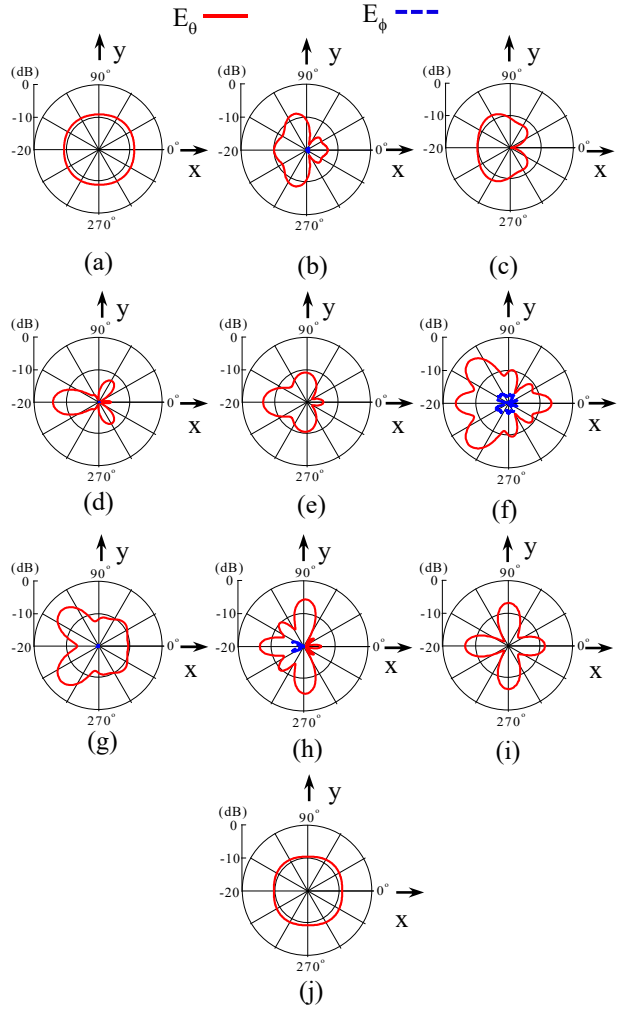


Fig. 15. Radiation patterns in the x-y azimuth plane at 4.2 GHz, with the number of open-state T-shaped elements, $N_{op}$, as a parameter. Parameters (H = $T_{VER}$, $T_{HOR}$, $D_{UP}$, $D_{GP}$, $N_{op}$) = (13 mm, 5 mm, 70 mm, 150 mm, varied) and the parameters in Table I are used. (a) $N_{op}$ = 0. (b) $N_{op}$ = 1. (c) $N_{op}$ = 3. (d) $N_{op}$ = 5. (e) $N_{op}$ = 7. (f) $N_{op}$ = 9. (g) $N_{op}$ = 11. (h) $N_{op}$ = 13. (i) $N_{op}$ =15. (j) $N_{op}$ =16.

This article has been accepted for publication in a future issue of this journal, but has not been fully edited. Content may change prior to final publication. Citation information: DOI 10.1109/TAP.2017.2779558, IEEE Transactions on Antennas and Propagation



TABLE II. O/S-STATE

| $N_{op}$ \ T.no | 1 | 2 | 3 | 4 | 5 | 6 | 7 | 8 | 9 | 10 | 11 | 12 | 13 | 14 | 15 | 16 |
|---|---|---|---|---|---|---|---|---|---|---|---|---|---|---|---|---|
| 0 | S | S | S | S | S | S | S | S | S | S | S | S | S | S | S | S |
| 1 | S | S | S | S | S | S | S | S | O | S | S | S | S | S | S | S |
| 3 | S | S | S | S | S | S | S | O | O | O | S | S | S | S | S | S |
| 5 | S | S | S | S | S | S | O | O | O | O | O | S | S | S | S | S |
| 7 | S | S | S | S | S | O | O | O | O | O | O | O | S | S | S | S |
| 9 | S | S | S | S | O | O | O | O | O | O | O | O | O | S | S | S |
| 11 | S | S | S | O | O | O | O | O | O | O | O | O | O | O | S | S |
| 13 | S | S | O | O | O | O | O | O | O | O | O | O | O | O | O | S |
| 15 | S | O | O | O | O | O | O | O | O | O | O | O | O | O | O | O |
| 16 | O | O | O | O | O | O | O | O | O | O | O | O | O | O | O | O |

T-shaped elements are in S-state; $N_{op}$ = 1 describes a situation where only T-shaped element 9 is in O-state; $N_{op}$ = 3 describes a situation where three T-shaped elements 9 and 9 ± 1 are in O-state; $N_{op}$ = 5 describes a situation where five T-shaped elements 9, 9 ± 1, and 9 ± 2 are in O-state; … ; $N_{op}$ = 16 describes a situation where all T-shaped elements 9, 9 ± 1, 9 ± 2, 9 ± 3, …., 9 ± 7 and 1 are in O-state. The T-shaped elements other than the open-circuited T-shaped elements are short-circuited to the ground plane. It is found that the radiation for $N_{op}$ = 5 is most directive with small backward radiation in the positive x-direction.

The radiation patterns in the x-z elevation plane for $N_{op}$ = 5 and $N_{op}$ = 16 are shown in Fig. 16, where $N_{op}$ = 16 means that all T-shaped elements are in O-state, as described above. Comparison of the radiation pattern in Fig. 16 (a) with that in Fig. 16(b) shows that the eleven S-state T-shaped elements behind the five O-state T-shaped elements contribute to reducing the backward radiation (in the positive x-direction) generated from both the five O-state T-shaped elements and the feed probe. In other words, the eleven T-shaped elements in S-state behave as a reflector.

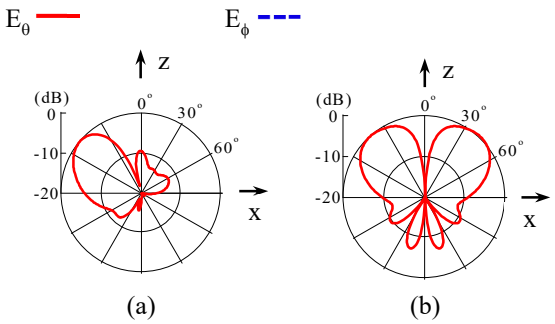


Fig. 16. Comparison of the radiation patterns in the x-z elevation plane at 4.2 GHz. Parameters (H = $T_{VER}$, $T_{HOR}$, $D_{UP}$, $D_{GP}$, $N_{op}$) = (13 mm, 5 mm, 70 mm, 150 mm, varied) and the parameters in Table I are used. $E_\phi$ does not appear. (a) $N_{op}$ = 5. T-shaped elements (7, 8, 9, 10, 11) are in O-state. (b) $N_{op}$ = 16. All T-shaped elements are in O-state.

## V. Experimental Work

### A. Manual operation for open- and short-circuited elements

Based on the investigations in section IV, an O-RadWG/Ts system is fabricated, where the parameters in Table I and (H = $T_{VER}$, $T_{HOR}$, $D_{UP}$, $D_{GP}$, $N_{op}$) = (13 mm, 5 mm, 70 mm, 150 mm, 5) are used with O-state T-shaped elements (7, 8, 9, 10, 11).

Fig. 17 (a) shows the fabricated antenna, where the UP denotes the open upper round plate for a radial waveguide, which is made of an aluminium film. The parasitic T-shaped element is made of a cupper film. The UP and T-shaped elements are supported by polystyrene form (relative permittivity $\varepsilon_r \approx 1$). The ground plane (GP) is made of an aluminium film. A vertical wire, connected to the inner conductor of a 50-ohm coaxial line, passes through the polystyrene form and is connected to the center point of the UP to activate the radial waveguide.

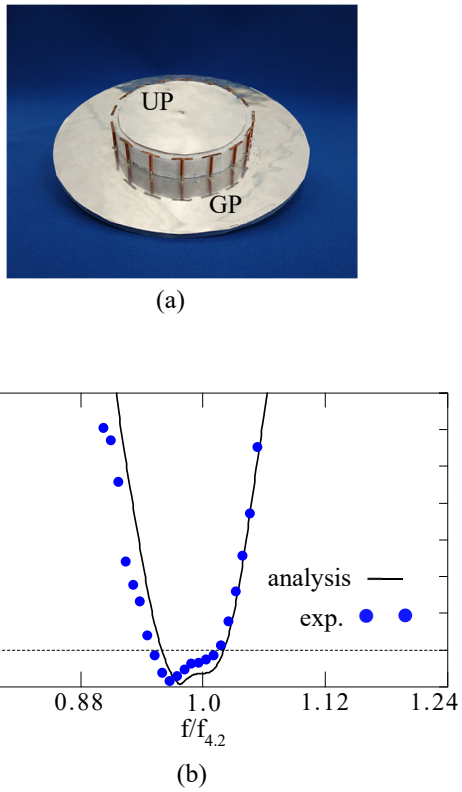


Fig. 17. (a) Fabricated O-RadWG/Ts, where UP denotes the open upper round plate for a radial waveguide. Images of T-shaped elements are seen in the ground plane (GP). (b) Frequency response of the VSWR, where parameters (H = $T_{VER}$, $T_{HOR}$, $D_{UP}$, $D_{GP}$, $N_{op}$) = (13 mm, 5 mm, 70 mm, 150 mm, 5) and the parameters shown in Table I are used. The bottom end of T-shaped elements (7, 8, 9, 10, 11) is open-circuited. $f_{4.2}$ denotes 4.2 GHz.

Note that the O-state situation is approximated by introducing an air gap of 0.1 mm between the end of T-shaped element and the ground plane; the S-state situation is obtained

This article has been accepted for publication in a future issue of this journal, but has not been fully edited. Content may change prior to final publication. Citation information: DOI 10.1109/TAP.2017.2779558, IEEE Transactions on Antennas and Propagation



by connecting the end of T-shaped element to the ground plane using silver paste.

Fig. 17(b) shows the frequency response of the VSWR. The bandwidth for a VSWR = 2 criterion is approximately 6%, which is suitable for narrow band communications. The experimental results confirm the analysis/simulation results of the VSWR. Confirmation is also found in Fig. 18, where the radiation pattern at frequencies around the design frequency 4.2 GHz is presented. The cross-polarization component $E_\phi$ is small relative to the co- polarization component $E_\theta$.

The beam direction is less sensitive to frequency, with a value of approximately ($\theta$, $\phi$) = (50°, 180°). Hence, the gain in the beam direction is also expected to be less sensitive. This is confirmed in Fig. 19.

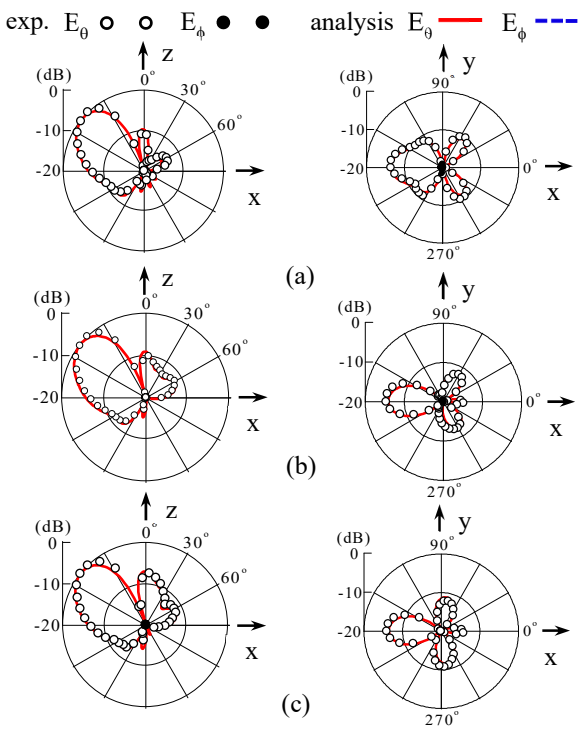


Fig. 18. Frequency response of the radiation pattern. Parameters (H = $T_{VER}$, $T_{HOR}$, $D_{UP}$, $D_{GP}$, $N_{op}$) = (13 mm, 5 mm, 70 mm, 150 mm, 5) and the parameters shown in Table I are used. The bottom end of T-shaped elements (7, 8, 9, 10, 11) is open-circuited. $E_\phi$ is small and does not appear on this scale. (a) f = 4.1 GHz = 0.976$f_{4.2}$. (b) f = 4.2 GHz = 1$f_{4.2}$. (c) f = 4.3 GHz = 1.023$f_{4.2}$.

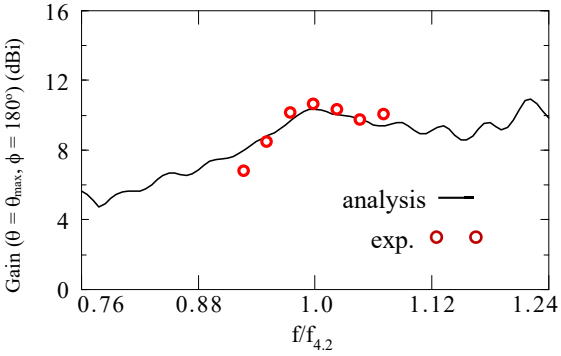


Fig. 19. Frequency response of the gain in the beam direction, where parameters (H = $T_{VER}$, $T_{HOR}$, $D_{UP}$, $D_{GP}$, $N_{op}$) = (13 mm, 5 mm, 70 mm, 150 mm, 5) and the parameters shown in Table I are used. The bottom end of T-shaped elements (7, 8, 9, 10, 11) is open-circuited. $f_{4.2}$ denotes 4.2 GHz.

## *B. Electronic Operation*

Fig. 20(a) shows the block diagram for electronic operation of the O-RadWG/Ts, whose upper round plate and T shaped elements are made of copper material. A GaAS MMIC based single pole single throw (SPST) failsafe switch [22] makes O-state and S-state. Fig. 20(b) shows switch control circuits printed on the surface of an FR4 dielectric substrate (relative permittivity $\varepsilon_r$ = 4.3 and thickness B = 1.6 mm). One port of the switch is connected to the T-element (T) and other port is contacted to the ground plane. A small single board digital computer, Raspberry Pi3 [23] provides the supply voltage (VDD) of 3.3 V and a switching control voltage (Vctl) of 3.2 V to the switching circuit. When Vctl = 0 V, the switch is 'off' and provide an O-state (reflective open) between the two switching ports. The switch is 'on' when Vctl = 3.2 V and provides an S-state between the ground plane and T-element. The switching control voltages are controlled by a GUI (Graphical User Interface) developed using Python programming language. The GUI laptop and the Pi are connected using a WiFi wave.

Figs. 21, 22, and 23 show the VSWR, radiation pattern, and gain, respectively. The measured results are close to the analysis/simulation results. The gain at the design frequency 4.2 GHz is 9.12 dBi, meeting the requirement in this paper. The gain reduction from the analysis/simulation value is approximately one dB, due to switching loss.

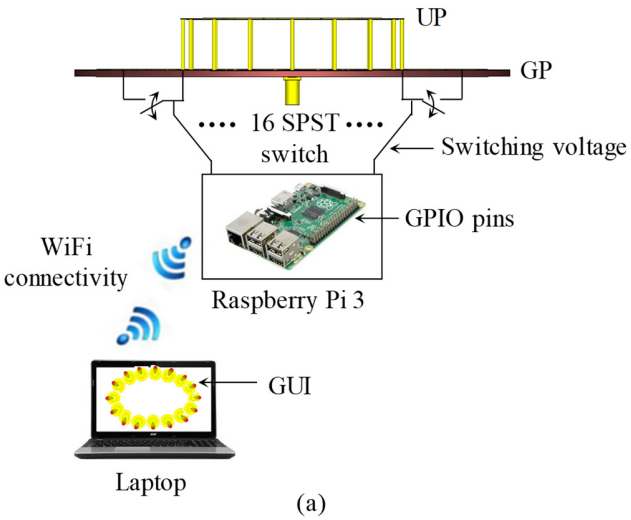

This article has been accepted for publication in a future issue of this journal, but has not been fully edited. Content may change prior to final publication. Citation information: DOI 10.1109/TAP.2017.2779558, IEEE Transactions on Antennas and Propagation



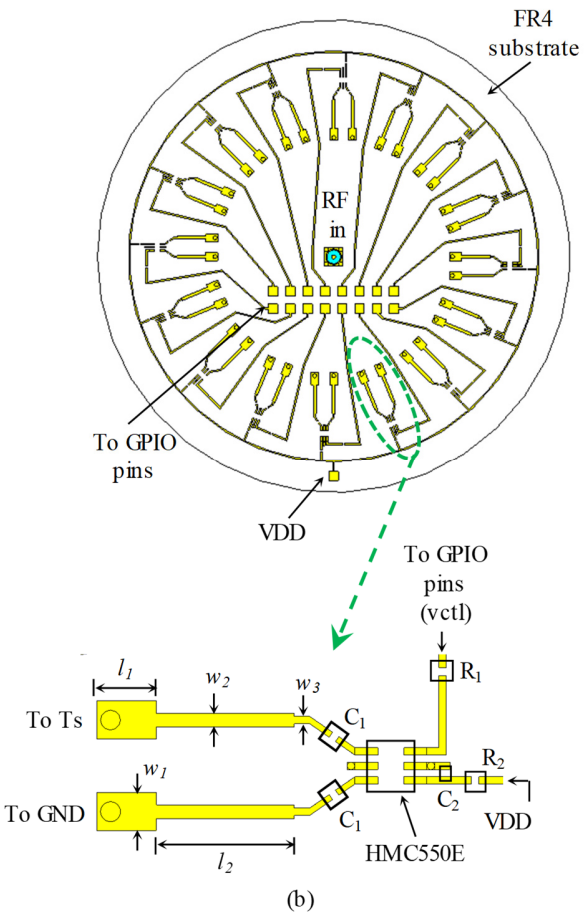


(b)

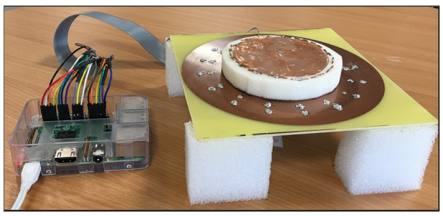

Antenna interfaced with the Raspberry pi 3

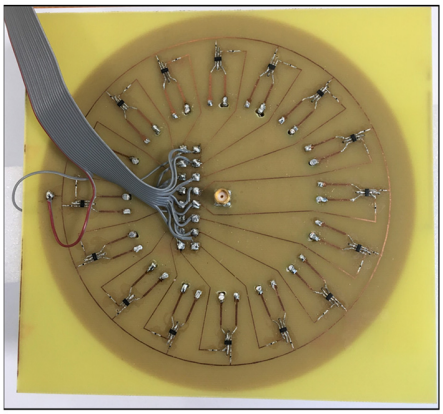

Bottom view of the switching circuit

(c)

Fig. 20. Electronic control of beam. (a) Block diagram. (b) On/Off circuit. (c) Photo of On/OFF circuit. The notations are as follows. UP: upper plate, GP: ground plane, GUI: Graphical User Interface, GPIO: General-purpose input/output, VDD: Plus source for FET [MOS(FET) drain voltage], HMC550E: Ref [22]. $C_1$ = 100 pF, $C_2$ = 1000 pF, $R_1$ = $R_2$ = 100 Ω, $l_1$ = 3.9 mm, $w_1$ = 2.5 mm, $l_2$ = 9 mm, $w_2$ = 0.9 mm, and $w_3$ = 0.48 mm. T-shaped elements are within polystyrene form and invisible.

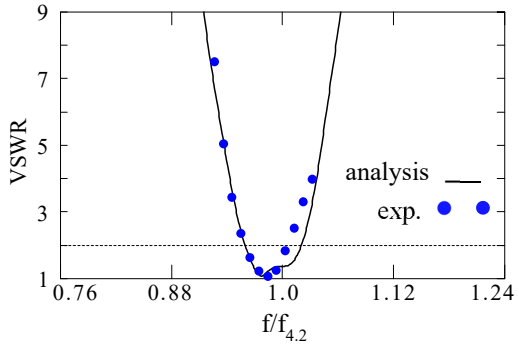


Fig. 21. Frequency response of the VSWR. The bottom end of T-shaped elements (7, 8, 9, 10, 11) is open-circuited. $f_{4.2}$ denotes 4.2 GHz.

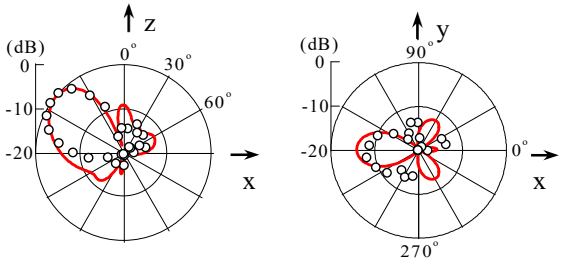


Fig. 22. Radiation pattern at design frequency of 4.2 GHz. The bottom end of T-shaped elements (7, 8, 9, 10, 11) is open-circuited.

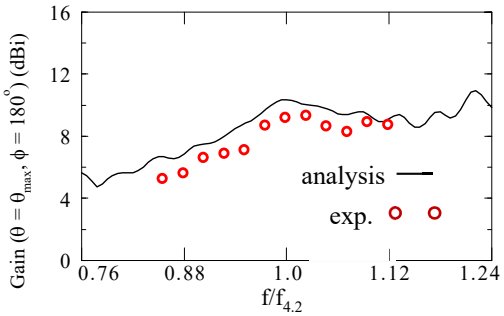


Fig. 23. Frequency response of the gain. The bottom end of T-shaped elements (7, 8, 9, 10, 11) is open-circuited. $f_{4.2}$ denotes 4.2 GHz.

This article has been accepted for publication in a future issue of this journal, but has not been fully edited. Content may change prior to final publication. Citation information: DOI 10.1109/TAP.2017.2779558, IEEE Transactions on Antennas and Propagation



## VI. State of T-Shaped Elements for Beam-Steering

The O-RadWG/Ts is symmetric with respect to the z-axis and hence the beam direction $\phi$ is varied by selecting O-state T-shaped elements: $\phi = 0^o$ for O-state elements (15, 16, 1, 2, 3), $\phi = 22.5^o$ for O-state elements (16, 1, 2, 3, 4), …., $\phi = 337.5^o$ for O-state elements (14, 15, 16, 1, 2). Fig. 24 illustrates the analysis result of variation in the beam direction provided by selected O-state elements. Each beam has a high gain of greater than the targeted gain 9 dBi, while maintaining the same radiation pattern and VSWR characteristics, i.e., the O-RadWG/Ts is a reconfigurable antenna.

## VII. Conclusions

A novel reconfigurable antenna system based on electromagnetic proximity-coupling has been proposed to meet three requirements: (i) a small antenna height, desired to be smaller than one-quarter wavelength ($\lambda/4$), (ii) a constant high gain of greater than 9 dBi in multi-direction across an azimuth range of $0^o \leq \phi \leq 360^o$ at a fixed elevation angle $\theta$, and (iii) a simple structure, not using reactive loads or phase shifters for beam steering.

Firstly, the design process and radiation mechanism for a reconfigurable antenna using electromagnetic proximity-coupling are explained. Secondly, an evolution process to an O-RadWG/Ts system, composed of an activated radial waveguide and parasitic T-shaped elements, is presented. It is revealed that the upper round plate for the radial waveguide provides constructive effects on the radiation pattern, gain, and VSWR. Reducing the side lobes and narrowing the beam width lead to a gain increase. Thirdly, effects of four major antenna system parameters on the antenna characteristics are investigated: antenna height H, upper round plate diameter $D_{UP}$, ground plane diameter $D_{GP}$, and number of T-shaped elements in open state, $N_{op}$. It is found that the VSWR for $0.15\lambda < H < \lambda/4$ remains almost unchanged. As $D_{UP}$ is increased, the VSWR band shifts toward a lower frequency region. Further findings are as follows; as $D_{GP}$ is increased, the beam direction moves toward the horizontal direction ($\theta = 90^o$); the beam is most directive when $N_{op} = 5$.

Based on these results, fourthly, an O-RadWG/Ts system is fabricated and measured. Good agreement between the analysed and measured results is obtained. A targeted gain of greater than 9 dBi in sixteen directions around the system axis (with an angle interval of 22.5°) is realized at the design frequency 4.2 GHz. The bandwidth for a VSWR = 2 criterion is approximately 6%. Thus, the measurement ensures that the O-RadWG/Ts system can steer the beam by selecting the state of the end of T-shaped elements (either opened or shorted to the ground plane, not using reactive loads).

## Acknowledgment

The authors thank V. Shkawrytko for his assistance in the preparation of this manuscript.

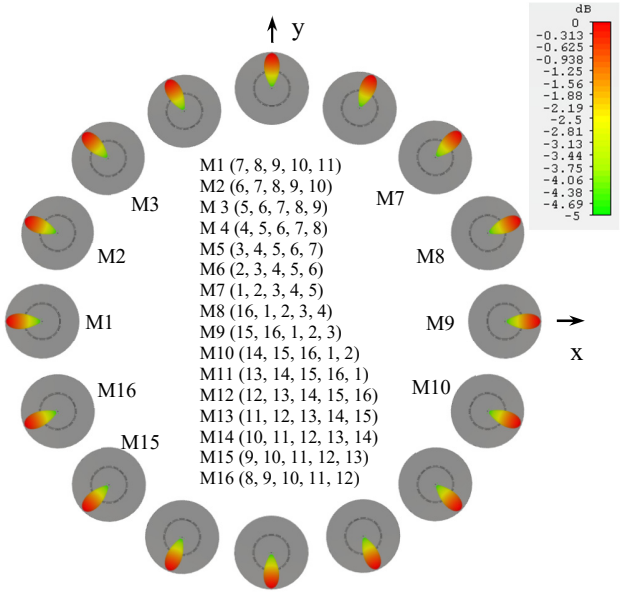


Fig. 24. Analysis/simulation result of sixteen steered beams with a $\phi$ = 22.5° interval at 4.2 GHz. Parameters (H = $T_{VER}$, $T_{HOR}$, $D_{UP}$, $D_{GP}$, $N_{op}$) = (13 mm, 5 mm, 70 mm, 150 mm, 5) and the parameters shown in Table I are used.

## References

[1] R. F. Harrington, "Reactivatedly controlled directive array," IEEE Trans. Antennas Propagat., vol. AP-26, no. 3, pp. 390-395, May1978.

[2] R. Vaughan, "Switched parasitic elements for antenna diversity," IEEE Trans. Antennas Propagat., vol. 47, no. 2, pp. 399-405, Feb. 1999.

[3] N. Scott, M. Leonard-Taylor, R. Vaughan, "Diversity gain from a single-port adaptive antenna using switched parasitic elements illustrated with a wire and monopole prototype," IEEE Trans. Antennas Propagat., vol. 47, no. 6, pp. 1066-1070, June 1999.

[4] T. Ohira and K. Gyoda, "Electronically steerable passive array radiator antennas for low-cost analog adaptive beamforming," Proc. IEEE Int. Conf. Phased Array Systems and Technology, pp. 101-104, 2000.

[5] K. Gyoda and T. Ohira, "Design of electronically steerable passive array radiator (ESPAR) antennas," IEEE AP-S Sym., vol.2, pp. 922-925, 2000.

[6] H. Kawakami and T. Ohira, "Electrically steerable passive array radiator (ESPAR) antennas," IEEE Antennas and Propagation Magazine, vol. 47, pp. 43-50, 2005.

[7] K. Murata, K. Iwata, H. Tsuboi, Y. Fukuda, N. Oki, H. Mimaki, and H. Nakano, "Beam scan antenna," Proc. IEICE General Conference, p. B-1-155, Osaka, March 2005.

[8] H. Nakano, R. Aoki, R. Kobayashi, and J. Yamauchi, "A patch antenna surrounded by parasitic Y elements for beam scanning,"

IEEE AP-S Int. Sym., vol. 3, pp. 2317-2320, Albuquerque, July 2006.

[9] H. Nakano, H. Honma, H. Umetsu, and J. Yamauchi, "A small steerable-beam antenna," ISAP, pp. 1-4, Singapore, November 2006.

[10] M. R. Kamarudin, P.S. Hall, F. Colombel, and M. Himdi, "CPW fed disc-loaded monopole array antenna with integrated PIN diode switches," iWAT, pp. 396-399, Cambridge, March 2007.

[11] Z. Shi, R. Zheng, J. Ding, and C. Guo, "A novel pattern-reconfigurable antenna using switched printed elements," IEEE Antennas Wireless Propagat. Lett., vol. 11, pp. 1100-1103, 2012.

[12] Y. Juan, W. Che, W. Yang, and Z. Chen, "Compact pattern-reconfigurable monopole antenna using parasitic strips," IEEE Antennas Wireless Propagat. Lett., issue 99, 2016.

[13] H. Liu, S. Gao, and T. H. Loh, "Electrically small and low cost smart antenna for wireless communication," IEEE Trans. Antennas Propagat., vol. 60, no.3, pp. 1540-1549, 2012.

[14] H. Liu, S. Gao, and T. H. Loh, "Compact MIMO antenna with frequency reconfigurability and adaptive radiation patterns," IEEE Antennas Wireless Propagat. Lett., vol.12., pp. 269-272, 2013.

## Appendix

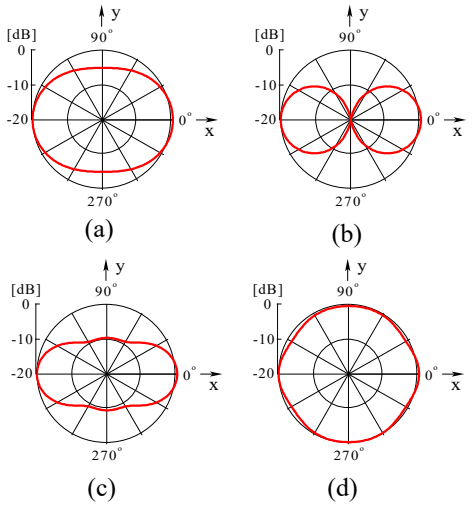


Fig. 25. Array factor for $N_{ac}$ activated elements at a design frequency of 4.2 GHz, where $N_{ac} = 2m + 1$. Parameters $D_T/2 = 37$ mm and $\Theta = 22.5^o$ are used. (a) m =1. (b) m = 2. (c) m = 3. (d) m = 4.

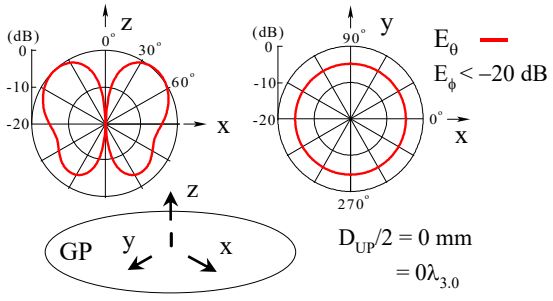


[15] Y. Y. Bai, S. Xiao, C. Liu, X. Shuai, and B. Z. Wang, "Design of pattern reconfigurable antennas based on a two-element dipole array model," IEEE Trans. Antennas Propag. Vol. 61, no. 9, pp. 4867-4871, 2013.

[16] C. Jin, R. Li, A. Alphones and X. Bao, "Quarter-mode substrate integrated waveguide and its application to antennas design," IEEE Trans. Antennas Propag., vol.61, no.6, pp.2921-2928, Jun. 2013.

[17] S. J. Shi and W. P. Ding, "Radiation pattern reconfigurable microstrip antenna for WiMAX application," Electron. Lett., Vol. 51, no. 9, pp. 662-664, 2015.

[18] M. S. Alam and A. M. Abbosh, "Beam-steerable planar antenna using circular disc and four pin-controlled tapered stubs for WiMAX and WLAN applications," IEEE Antennas Wireless Propag. Lett., vol. 15, pp. 980-983, 2016.

[19] H. Nakano, *Low-profile natural and metamaterial antennas*, IEEE Press/ Wiley, 2016.

[20] R. F. Harrington, *Field Computation by Moment Methods*, Macmillan, New York, 1968.

[21] https://www.cst.com/applications/mwandrf.

[22] http://www.analog.com/media/en/technical-documentation/data-sheets/hmc550.pdf.

[23] https://www.raspberrypi.org/products/raspberry-pi-3- model-b/.

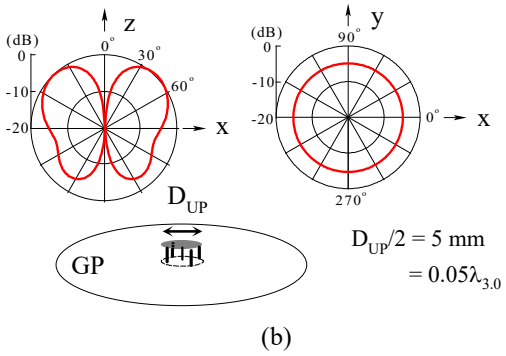


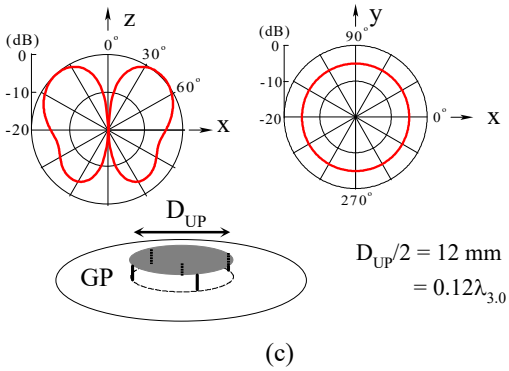

This article has been accepted for publication in a future issue of this journal, but has not been fully edited. Content may change prior to final publication. Citation information: DOI 10.1109/TAP.2017.2779558, IEEE Transactions on Antennas and Propagation



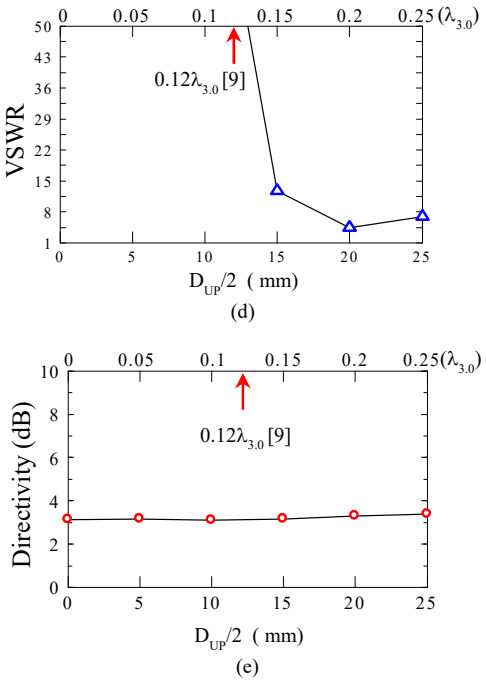


Fig. 26. Inner section of Small Shorting-Disc/Ts[9], designated as the Small Shorting-Disc Monopole Antenna, where the central fed monopole height is 8 mm and other parameters are: frequency f = 3 GHz (wavelength $\lambda_{3.0}$ = 100 mm), ground plane (GP) diameter $D_{GP}$ = 100 mm, and central fed monopole diameter $2a_F$ = 1 mm. (a)-(c) Radiation pattern. (d) VSWR. (e) Directivity.

**Hisamatsu Nakano** (M'75–SM'87–F'92–LF'11) has been with Hosei University since 1973, where he is now a professor emeritus and a special-appointment researcher at the *Electromagnetic Wave Engineering Research Institute* attached to the graduate school of the same university. His research topics include numerical methods for low- and high-frequency antennas and optical waveguides. He has published over 300 articles in major journals and 11 books/book-chapters, including "*Low-profile Natural and Metamaterial Antennas* (IEEE Press, Wiley)." His significant contributions are the development of five integral equations for line antennas and the realization of numerous wideband antennas, including curl, spiral, helical, and cross-wire antennas. His other accomplishments include antennas for GPS, personal handy phone, space radio, electronic toll collection, RFID, UWB, and radar. He has been awarded 78 patents, including *A Curl Antenna Element and Its Array* (Japan). He has held the positions of Visiting Associate Professor at Syracuse University (March to September, 1981), Visiting Professor at the University of Manitoba (March to September, 1986), University of California, Los Angeles (September, 1986 to March, 1987), and Swansea University, UK (June to September, 2016 and July to October, 2017). Prof. Nakano received the "*H. A. Wheeler Award"* in 1994, "*Chen-To Tai Distinguished Educator Award"* in 2006, and "*Distinguished Achievement Award*" in 2016, all from IEEE ANTENNAS AND PROPAGATION SOCIETY. He was also the recipient of "*The Prize for Science and Technology*" from Japan's Minister of Education, Culture, Sports, in 2010. Prof. Nakano is an Associate Editor of several journals and magazines, such as Electromagnetics and the IEEE Antennas and Propagation Magazine. He served as a member of the IEEE APS administrative committee (2000-2002) and a Region 10 Representative (2001-2010).

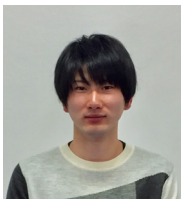

**Yuhei Kameta** was born in Ibaraki, Japan, on January 30, 1994. He received the B.E. degree in electronics and electrical engineering from Hosei University, Tokyo, Japan, in 2016. Mr. Kameta is a member of the Institute of Electronics, Information and Communication Engineers of Japan.

**Tour Kawano** (M'97) was born in Oita, Japan, on December 26, 1971. He received the B.E., M.E., and Dr. E. degrees in electrical engineering from Hosei University, Tokyo, Japan, in 1995, 1997, and 2001, respectively. From 2001 to 2010, he was an assistant with the National Defense Academy of Japan, Kanagawa, Japan. He is currently a Lecturer at the National Defense Academy. His current research interests are antennas, scattering, and propagation of electromagnetic waves. He is a member of the Institute of Electronics, Information and Communication Engineers of Japan.

**Amit Mehta** (M'05 - SM'11) received the B.Eng. degree in electronics and telecommunication from the University of Pune, India, in 1998 and the M.Sc. degree in telecommunications and information networks and the Ph.D. degree in smart reconfigurable antennas from the University of Essex, U.K., in 2002 and 2005, respectively. From 1998 to 2001, he worked in the Telecommunications Industry in Bangalore and Singapore. From July 2002 to February 2006, he was a Senior Research Officer at the University of Essex. Since February 2006, he has been working at Swansea University, Swansea, U.K. and is the director of the RF research group where his core research focus is wireless communications, microwave systems and antennas. He is particularly interested in GNSS, body-wearable adaptable antennas, satellite communications, smart antennas, 4G, and millimeter waves. He has successfully supervised over 20 postgraduate research theses and has over 80 technical publications and three patents on invention of the steerable beam smart antenna and concealed weapons detection system.

**Arpan Pal** (M'09) received the Ph.D. degree in advanced telecommunications from Swansea University, Swansea, U.K., in 2013. He worked as a Research Assistant at the Indian Institute of Science (IISc), Bangalore, India, from 2005 to 2006 and at Swansea University, in 2008. Thereafter, he worked as a Lecturer at the Asansol Engineering College, West Bengal, India. In 2014, he was a Research Assistant at The Institute of Electronics Communications and Information Technology (ECIT), Queen's University of Belfast, Belfast, U.K. Since December 2014, he has been a Research Assistant at Antenna and Smart City Lab, Swansea University, U.K. His research interest

involves beam-steerable antennas, phased array antennas, frequency selective surface and surface-integrated waveguide antennas.

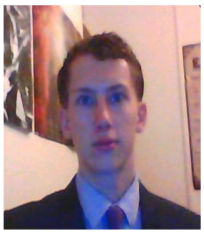

**Andrew Skippins** was born in West Wales, United Kingdom, in August, 1994. He completed the BEng degree in Electronics and Electrical Engineering, and MSc Communications Engineering in 2016 and 2017, respectively, from Swansea University, UK. He is currently working as a research assistant in the Antenna and Smart City Lab, Swansea University. Mr Skippins is a member of the Institute of Engineering and Technology.

**Junji Yamauchi** (M'84–SM'08–F'12) was born in Nagoya, Japan, on August 23, 1953. He received the B.E., M.E., and Dr. E. degrees from Hosei University, Tokyo, Japan, in 1976, 1978, and 1982, respectively. From 1984 to 1988, he served as a Lecturer in the Electrical Engineering Department, Tokyo Metropolitan Technical College. Since 1988, he has been a member of the faculty of Hosei University, where he is now a Professor at the Electronics and Electrical Engineering Department. His research interests include optical waveguides and circularly polarized antennas. He is the author of the book Propagating Beam Analysis of Optical Waveguides (Research Studies Press, 2003). Dr. Yamauchi is a member of the Optical Society of America and the Institute of Electronics, Information and Communication Engineers of Japan.